Author Manuscript

Author Manuscript

Author Manuscript

Author Manuscript

HHS Public Access

Author manuscript

Magn Reson Med. Author manuscript; available in PMC 2016 September 01.

Published in final edited form as:

Magn Reson Med. 2015 September ; 74(3): 785–802. doi:10.1002/mrm.25457.

Bayesian Analysis of Transverse Signal Decay with Application to Human Brain

Mustapha Bouhrara, **David A. Reiter**, and **Richard G. Spencer***

Laboratory of Clinical Investigation, National Institute on Aging, National Institutes of Health, Baltimore, MD 21224, USA

Abstract

Purpose: Transverse relaxation analysis with several signal models has been used extensively to determine tissue and material properties. However, the derivation of corresponding parameter values is notoriously unreliable. We evaluate improvements in the quality of parameter estimation using Bayesian analysis and incorporating Rician noise, as appropriate for magnitude MR images.

Theory and Methods: Monoexponential, stretched exponential, and biexponential signal models were analyzed using nonlinear least squares (NLLS) and Bayesian approaches. Simulations, and phantom and human brain data, were analyzed using three different approaches to account for noise. Parameter estimation bias, reflecting accuracy, and dispersion, reflecting precision, were derived for a range of signal-to-noise ratios (SNR) and relaxation parameters.

Results: All methods performed well at high SNR. At lower SNR, the Bayesian approach yielded parameter estimates of considerably greater precision, as well as greater accuracy, than did NLLS. Incorporation of Rician noise greatly improved accuracy and, to a somewhat lesser extent, precision, in derived transverse relaxation parameters. Analyses of data obtained from solution phantoms and from brain were consistent with simulations.

Conclusion: Overall, estimation of parameters characterizing several different transverse relaxation models was markedly improved through use of Bayesian analysis and through incorporation of Rician noise.

Keywords

Bayesian probability; Nonlinear least squares algorithm; Transverse relaxation; Brain; Accuracy; Precision; Rician noise

INTRODUCTION

Relatively little work has been undertaken to evaluate the Bayesian probability approach to parameter estimation from noisy MR images. In particular, the performance of Bayesian as compared to nonlinear least squares (NLLS) analysis in the quantification of transverse decay, as described by monoexponential and alternative models, has not been reported. However, these models are of increasing interest in both preclinical and clinical studies in

*Address correspondence to: Richard G. Spencer, M.D., Ph.D., NIH/National Institute on Aging, Intramural Research Program, BRC 04B-116, 251 Bayview Boulevard, Baltimore, MD 21224, USA., Tel: 410-558-8226, spencer@helix.nih.gov.

Author Manuscript Author Manuscript Author Manuscript Author Manuscript

order to characterize tissue ultrastructure, identify tissue compartments, and differentiate between normal and pathologic tissues.

Multiexponential transverse relaxation analysis (METRA) (1-7) is one approach to this type of characterization, in which extraction of transverse relaxation times and component amplitudes from relaxation data is achieved through use of the inverse Laplace transform (ILT). This is typically implemented through the NLLS or the nonnegative least square algorithms. However, the ill-posed nature of the ILT makes the inversion very sensitive to noise (8-9), rendering parameter estimation difficult, especially in the clinical setting.

It has been demonstrated that explicitly incorporating the Rician noise model appropriate to magnitude magnetic resonance (MR) images (10-11) greatly improves accuracy and precision in derived parameter estimates (12-14), including for biexponential signals (15). Despite this, bias and dispersion resulting from application of NLLS increase substantially with decreasing SNR or with increasing disparity between component sizes (15-16).

Parameter estimation using Bayesian probability theory has long been recognized as having several advantages over NLLS minimization (17-18), including the fact that it does not require initial estimates. In addition, the estimate of a given parameter is derived through integration, or marginalization, over the probability distribution functions (PDFs) of the remaining parameters. The resulting PDF of the parameter of interest, the so-called posterior PDF, is therefore not influenced by local minima of a global fitting function defined by multiple parameters as is the case for NLLS (19). The posterior PDF completely defines the uncertainty in the derived parameter estimate (20). Among other benefits, this permits assessment of MR parameter uncertainty within a single voxel (21).

While laying a foundation for Bayesian analyses of MR data, these previous results were restricted to NMR spectroscopic data or to monoexponential transverse decay over a restricted parameter range. In the present work, our goal is to provide a much more comprehensive evaluation of the quality of parameter estimation from transverse relaxation imaging data through use of Bayesian analysis as compared to NLLS. Analyses were performed using the appropriate Rician noise model, as that has been clearly demonstrated to provide improved estimates as compared to the Gaussian noise approximation (12-15, 21). Three distinct signal relaxation models were studied, the monoexponential, stretched exponential, and biexponential, over a large range of parameters and SNR values. All three of these models are used in the analysis of complex systems.

We first review the theory of noise distribution in MR images. We then describe in detail the six different voxel-by-voxel fitting methods we compared, three based on NLLS minimization and three based on Bayesian analysis. Next, extensive Monte Carlo (MC) simulations are presented which give the relative bias and dispersion in the estimation of transverse relaxation parameters using the six methods. Finally, we present data obtained from phantoms at 7 Tesla (T) and from human brain at 3T.

Author Manuscript Author Manuscript Author Manuscript Author Manuscript

THEORY

MRI Signal Distribution

The PDF of magnitude imaging data **S** = $\{S_n\}$ measured at echo times $TE_n = n * TE$ defined by echo time *TE* and echo number *n*, with Gaussian-distributed noise of equal variance, σ^2, in the real and imaginary channels, is given by the Rician distribution (10):

$$P_{Rice}\left(S_n|A\left(\theta;\mathbf{TE_n}\right),\sigma\right)=\frac{S_n}{\sigma^2}exp\left(-\frac{A^2\left(\theta;\mathbf{TE_n}\right)+S_n^2}{2\sigma^2}\right)I_0\left(\frac{A\left(\theta;TE_n\right)S_n}{\sigma^2}\right)u\left(S_n\right) \quad [1]$$

where $A(\theta;TE_n)$, is the magnitude of the underlying noise-free signal as a function of TE_n and signal parameters θ, I_k is the modified *k*-order Bessel function of the first kind and *u* is the Heaviside step function. The first moment, or expectation value, of the Rician PDF is given by (22-23)

$$\begin{aligned}E_{Rice}\left[S_n\right]&=\int_0^{\infty}S_nP_{Rice}\left(S_n|A\left(\theta;TE_n\right),\sigma\right)dS_n\\&=\sigma\sqrt{\frac{\pi}{2}}exp\left(-\frac{\phi_n}{2}\right)+\left(\left(1+\phi_n\right)I_0\left(\frac{\phi_n}{2}\right)+\phi_nI_1\left(\frac{\phi_n}{2}\right)\right)\end{aligned} \quad [2]$$

where $\phi_n = A^2(\theta;TE_n)/2\sigma^2$.

From Eq. 1, the likelihood function for the transverse decay data within a voxel is (24)

$$\begin{aligned}L_{Rice}\left(\mathbf{S}|\theta,\sigma\right)&=\prod_{n=1}^{N}P_{Rice}\left(S_n|A\left(\theta;\mathbf{TE_n}\right),\sigma\right)\\&=\frac{1}{\sigma^{2N}}exp\left(-\frac{\Sigma_{n=1}^{N}\left(A^2(\theta;\mathbf{TE_n})+S_n^2\right)}{2\sigma^2}\right)\prod_{n=1}^{N}S_nI_0\left(\frac{A(\theta;\mathbf{TE_n})S_n}{\sigma^2}\right)\end{aligned} \quad [3]$$

At high SNR, $S_nA(\theta;TE_n) \gg \sigma^2$ so that $I_0(A(\theta;TE_n)S_n/\sigma^2)$ approaches $exp\left(S_nA\left(\theta;\mathbf{TE_n}\right)/\sigma^2\right)/\sqrt{2\pi S_nA\left(\theta;\mathbf{TE_n}\right)/\sigma^2}$. In this limit, the Rician PDF approximates the Gaussian distribution with mean $A(\theta;TE_n)$ and variance σ^2 (11, 25):

$$P_{Gauss}\left(S_n|A\left(\theta;\mathbf{TE_n}\right),\sigma\right)=\frac{1}{\sigma\sqrt{2\Pi}}exp\left(-\frac{\left(A\left(\theta;\mathbf{TE_n}\right)-S_n\right)^2}{2\sigma^2}\right)u\left(S_n\right) \quad [4]$$

with first moment, or expectation value, given by

$$E_{Gauss}\left[S_n\right]=\int_{-\infty}^{+\infty}S_nP_{Gauss}\left(S_n|A\left(\theta;\mathbf{TE_n}\right),\sigma\right)dS_n=A\left(\theta;\mathbf{TE_n}\right) \quad [5]$$

From Eq. 4, the Gaussian likelihood function of the imaging data **S** is

Author Manuscript Author Manuscript Author Manuscript Author Manuscript

$$L_{Gauss}\left(\mathbf{S}|\theta,\sigma\right)=\prod_{n=1}^{N}P_{Guass}\left(S_n|A\left(\theta;TE_n\right),\sigma\right)$$
$$=\frac{1}{(2\pi\sigma^2)^{N/2}}exp\left(-\frac{\Sigma_{n=1}^{N}(A(\theta;\mathbf{TE_n})-S_n)^2}{2\sigma^2}\right) \quad [6]$$

NLLS and Bayesian Parameter Estimation Approaches

NLLS parameter estimation is generally rapid and accurate for low dimensional problems, that is, those for which the number of parameters to be estimated is small. However, in higher dimensions, NLLS estimation is greatly complicated by the presence of local minima; this difficulty increases with model complexity, with an increasing number of free parameters to be determined, and with decreasing SNR (19).

Bayesian analysis is an alternative approach that can be particularly robust for parameter estimation in the presence of noise (17, 20-21, 26-34). In this framework, parameter probability distributions are calculated from the observed data and prior knowledge. Bayesian parameter estimation is based on the posterior probability density of parameters, θ, given the observed data, **S**, and the standard deviation of the noise, σ. The formal statement of Bayes theorem in this context is (35-36):

$$\mathrm{P}\left(\theta|\mathbf{S},\sigma\right)=\frac{\mathrm{P}\left(\theta\right)L\left(\mathbf{S}|\theta,\sigma\right)}{\mathrm{P}\left(\mathbf{S}\right)} \quad [7]$$

where P(θ) represents an *a priori* parameter distribution based on pre-existing knowledge, L(**S**|θ,σ) is the likelihood function of **S** given θ and σ, and P(**S**) is a normalization constant, which corresponds to our use of normalized probability distributions.

The successive marginalization over all parameters results in a considerable computational burden, but permits the calculation of a posterior PDF for each individual parameter. An estimate $\hat{\theta}_i$ can be derived from the PDF of θ_i in several ways. It can be taken as the mean of the PDF P(θ_i|**S**,σ), as is widely used in statistical inference, or as its median value. In this paper, we define $\hat{\theta}_i$ as the maximum posterior probability (MAP), as is common in Bayesian image analysis (37):

$$\hat{\theta}_i=\underset{\theta_i\in\theta}{argmax}\left\{\mathrm{P}\left(\theta_i|\mathbf{S},\sigma\right)\right\} \quad [8]$$

METHODS

Transverse Relaxation Signal Models

Monoexponential Signal—The monoexponential model implicitly assumes a single pool of water protons, leading to transverse decay of the form:

Author Manuscript Author Manuscript Author Manuscript Author Manuscript

$$A\left(\theta;\mathbf{TE_n}\right)=A_0 exp\left(-\frac{TE_n}{T_2}\right) \quad [10]$$

Thus, this model is characterized by the parameter pair $\theta = (A_0\ T_2)$, with A_0 representing the signal amplitude for $TE = 0$, incorporating T_1-weighting, proton density, coil sensitivity and other machine factors. T_2 represents the spin-spin relaxation time.

Stretched Exponential Signal—Biological tissues are characterized by a complex physicochemical structure (1-7, 38-41) so that the monoexponential function (Eq. 10), while often a useful approximation, would not be expected to account for important features of transverse relaxation (42). Therefore, alternative relaxation models that permit a more detailed description of the relationship between relaxation or diffusion processes and internal material structure have become of interest (43-47).

The stretched exponential decay model is given by

$$A\left(\theta;\mathbf{TE_n}\right)=A_0 exp\left(-\left(\frac{TE_n}{T_2}\right)^{\alpha}\right) \quad [11]$$

with parameters $\theta = (A_0\ g{=}a\ T_2;\ a \in (0,1]$ defines the deviation from monoexponential decay. This arises in several settings, including as an approximation to a continuous distribution of decay constants and in systems with memory as represented by fractional order processes (47).

Biexponential Signal—Restricting METRA to biexponential signals has been found to be a good approximation to transverse relaxation in a number of studies and is particularly appropriate in settings of only moderate SNR, such as is achievable clinically (48-51). For the case of two distinct proton pools that are not exchanging, the signal decay function is

$$A\left(\theta;\mathbf{TE_n}\right)=A_0\left(f_s exp\left(-\frac{TE_n}{T_{2,s}}\right)+\left(1-f_s\right) exp\left(-\frac{TE_n}{T_{2,l}}\right)\right) \quad [12]$$

with parameters $\theta = (A_0 f_s T_{2,s} T_{2,l})$, where f_s is the fraction of the short T_2 component, and $T_{2,s}$ and $T_{2,l}$ are the spin-spin relaxation times of the short-T_2 and long-T_2 components, respectively. It is well-known that derivation of accurate parameter values can be highly problematic (15-16) even for this simple biexponential signal model.

Parameter Estimation Methods

For each of the above three signal models, six methods of parameter estimation were implemented. They are defined by use of NLLS versus Bayesian analysis, and by signal models using Gaussian noise, Gaussian noise plus an offset, and Rician noise. More precisely, the first method, denoted $NLLS_G$, uses the Gaussian estimator in Eq. 5, and consists of NLLS minimization of $S_n - E_{Gauss}[S_n]$, that is, $S_n - A(\theta;TE_n)$, with $A(\theta;TE_n)$ defined by Eqs. 10-12. The second method evaluated, $NLLS_{G,O}$, uses the Gaussian estimator

Author Manuscript Author Manuscript Author Manuscript Author Manuscript

plus an offset ε, and consists of NLLS minimization of $S_n - (A(\theta;TE_n) + \varepsilon)$. This is the simplest method used to account for noise in magnitude reconstruction (52-54) (Fig. 1). The third method, $\mathrm{NLLS}_{\mathbf{R}}$, makes full use of the expectation value of the Rician distribution given by Eq. 2, and involves NLLS minimization of $S_n - E_{Rice}[S_n]$. The fourth method, $\mathrm{MAP}_{\mathrm{G}}$, is a Bayesian analysis using the Gaussian likelihood function, $L_{Gauss}(\mathbf{S}|\theta,\sigma)$, given by Eq. 6. The fifth parameter estimation method, $\mathrm{MAP}_{\mathrm{G,O}}$, is a Bayesian analysis using the Gaussian likelihood function, $L_{Gauss}(\mathbf{S}|\theta,\sigma)$, given by Eq. 6, but incorporating an offset, so that $(A(\theta;TE_n)$ is replaced by $(A(\theta;TE_n)$. The sixth method evaluated, $\mathrm{MAP}_{\mathbf{R}}$, is a Bayesian analysis using the Rician likelihood function, $L_{Rice}(\mathbf{S}|\theta,\sigma)$, given by Eq. 3. The marginalization process required in the Bayesian-based methods is described in the Appendix. All numerical calculations were performed using Matlab (MathWorks, Natick, MA, USA), with NLLS fits performed with the Levenberg-Marquardt algorithm.

Estimations of Standard Deviation, Variance and Offset of the Noise

We take the standard deviation, σ, variance, σ^2, and offset, ε, of the noise as known parameters. These were input values in our simulation studies, while in phantom and *in vivo* studies they were estimated from background regions in which $A(\theta;TE_n) = 0$ so that Eq. 1 reduces to the Rayleigh distribution (11, 55-56):

$$P_{Rayleigh}(S_n|\alpha) = \frac{S_i}{\sigma^2} exp\left(-\frac{S_n^2}{2\sigma^2}\right) \quad [13]$$

The first and the second moments of $P_{Rayleigh}(S_n|\sigma)$ are (57-58)

$$E_{Rayleigh}[S_n] = \int_0^\infty S_n P_{Rayleigh}(S_n|\sigma)\, dS_n = \sigma\sqrt{\frac{\pi}{2}} \quad [14]$$

and

$$E_{Rayleigh}\left[S_n^2\right] = \int_0^\infty S_n^2 P_{Rayleigh}(S_n|\sigma)\, dS_n = 2\sigma^2 \quad [15]$$

from which unbiased estimates of σ, σ^2 and ε may be obtained through

$$\hat{\sigma} \simeq \left(NK\sqrt{\pi/2}\right)^{-1} \Sigma_{n=1}^{N}\Sigma_{k=1}^{K} S_n^k, \quad \hat{\sigma^2} \simeq (2NK)^{-1}\Sigma_{n=1}^{N}\Sigma_{k=1}^{k}\left(S_n^k\right)^2 \quad and \quad \hat{\epsilon} \simeq \hat{\sigma}\sqrt{\pi/2}$$

(57-58), where K is the total number of voxels taken as background. Note that to improve the quality of these estimates, the signal-free regions were formed from the background intensity in all of the echo images.

Bias and Dispersion Calculations

For each method, the relative bias, a measure of accuracy, was defined from the difference between the true value, θ_i, and the mean of the estimated value, $\hat{\theta}_i$, by $100 * |\theta_i - (1/M)\,\Sigma_{m=1}^{M}\hat{\theta}_i^m|/\theta_i$. In simulations, M is the total number of noise realizations, while in phantom studies it is the total number of voxels for which parameter maps were

Author Manuscript Author Manuscript Author Manuscript Author Manuscript

generated. In simulations, true parameter values were known, while in phantom studies they were obtained from a monoexponential fit (12) of high SNR data acquired from each phantom compartment separately (see below). Note that the phantom studies were limited to the monoexponential and biexponential models. Relative dispersion, a measure of precision, was similarly defined by $100 * \sqrt{(1/M-1)\,\Sigma_{m=1}^{M}\left(\hat{\theta}_i^m - \theta_i^m\right)^2}/\theta_i$

Relative bias and dispersion were calculated after removal of voxels with extreme outliers (VEO) using Tukey's method (59) to correspond to actual practice (12, 15).

In contrast to simulations and phantom studies, exact parameter values for the brain were unknown so that relative bias and dispersion cannot be evaluated. Instead, relative error maps for each estimated parameter were calculated using $\mathrm{MAP}_{\mathbf{R}}$ analysis of high SNR imaging data as the reference, although we note that maps were essentially identical for all analysis methods using the high SNR data. For each estimated parameter, errors in the values obtained at lower SNR were calculated from the difference between the estimated value, $\hat{\theta}_i$, and its reference value, $\hat{\theta}_{i,ref}$, according to $error{=}100 * |\hat{\theta}_i - \hat{\theta}_{i,ref}|/\hat{\theta}_{i,ref}$.

In simulations, SNR was defined as $A(\boldsymbol{\theta};TE_n)/\sigma$, where TE_1 is the shortest echo time at which data were generated. In phantom and *in vivo* studies, it was defined as $\sqrt{\bar{S}\,(TE_1)^2 - 2\hat{\sigma}^2}/\hat{\sigma}$ (60), where $\bar{S}(TE_1)$ represents the mean signal calculated from a large region of the MR image obtained at TE_1.

Numerical Simulation Studies

MC simulations were performed using monoexponential (Eq. 10), stretched exponential (Eq. 11), and biexponential (Eq. 12) signal models for a wide range of underlying parameters and as a function of SNR, achieved through addition of Rician noise (Fig. 1). For all simulations, a total of 32 data points were generated with TE_n increasing uniformly from 8 to 256 ms. The required starting values needed in the NLLS analyses were set to their true values. For each signal model and for each set of parameters, relative bias and dispersion were calculated over 1000 noise realizations for each estimated parameter using the six analysis methods.

MC Simulations 1: Effect of SNR—MC simulations were performed to examine the effect of SNR on the relative bias and dispersion in derived parameters. The underlying true model parameters were chosen to reflect values obtained from the *in vivo* study of human brain (below).

For the monoexponential (Eq. 10), T_2 = 70 ms was used, with Rician noise added to achieve SNR ranging from 10 to 60 in increments of 10. For the stretched exponential (Eq. 11), T_2 = 60 ms and α = 0.8 were used, with SNR values ranging from 10 to 100 in increments of 10. For the biexponential analysis (Eq. 12), the underlying parameters were f_s = 0.25, $T_{2,s}$ = 20 ms and $T_{2,l}$ = 90 ms, with an SNR range of 30 to 120, again in increments of 10. The different SNR ranges were selected to account for the difference in complexity of these three signal models. For example, the SNR requirement for the monoexponential is less stringent

Author Manuscript Author Manuscript Author Manuscript Author Manuscript

than for the other two models, so lower values of SNR were appropriate for the analysis. The parameter estimates begin to break down severely at the lower limit of SNR, and became relatively stable at the higher value, in each case.

MC Simulations 2: Effect of Underlying Parameters—MC simulations were also used to explore the effect of underlying true parameter values on the relative bias and dispersion in derived parameters. The wide range of underlying parameters investigated is summarized in Fig. 3-5. Again, appropriate values of SNR were selected, with SNR of 10 and 50 for the monoexponential, 10 and 70 for the stretched exponential, and 30 and 100 for the biexponential.

Phantom Studies

Phantom studies were designed to validate the monoexponential and biexponential MC simulations. Three rectangular tubes (5 × 3 cm) filled with deionized water were doped with different concentrations of $CuSO_4$. The tubes were then placed together in the MRI system, and images were acquired using a 3D CPMG sequence (61-62) on a 7T small animal MRI scanner (Bruker Biospin GmbH, Rheinstetten, Germany) equipped with a linearly polarized birdcage coil. 35 T_2-weighted images with TE_n increasing linearly from 5.1 to 180 ms were acquired. Other imaging parameters included TR = 1000 ms, field of view (FOV) = 70 × 40 × 40 mm^3, and matrix = 140 × 80 × 20. Images were obtained with different numbers of signal averages, ranging from 1 to 8. Linear combinations of complex imaging data from each pair of phantoms were created and added with consistent phases to obtain Rician-distributed magnitude images with different compartment fractions (15). Relative bias and dispersion were calculated for each estimated parameter using the six analysis methods. Fiducial T_2 values were obtained from high SNR data acquired from each tube independently and fit to a monoexponential; they were 14 ± 2 ms, 58 ± 1 ms and 112 ± 3 ms from tubes 1, 2 and 3, respectively. These were used as initial estimates for the NLLS analysis.

Phantom Study 1: Effect of SNR—Images acquired from tube 2, with T_2 = 58 ms, were fit to a monoexponential using the six investigated methods. Data from the separate measurements on tube 1, with T_2 = 14 ms, and tube 3, with T_2 =112 ms, were constructed as described above in order to synthesize two-component images with f_s = 0.33 and with a range of SNR's. Each voxel from these composite images was fit to a biexponential function.

Phantom Study 2: Effect of Underlying Parameters—T_2 weighted images were fit to a monoexponential independently for each of the three imaged tubes. For the biexponential, different composite images were created with several f_s values and ratios $T_{2,l}/T_{2,s}$ (see Fig. 8). Fits were performed at two different SNR's, as indicated in Fig. 8.

In vivo Study

T_2-weighted images of the brain of a 40 year-old male volunteer were acquired with a 3T whole-body MRI system (Achieva, Philips Medical Systems) equipped with a quadrature head coil. 32 axial MR images were obtained using a 3D CPMG sequence with TE_n increasing linearly from 8 to 256 ms, TR = 700 ms, FOV = 240 × 240 × 15 mm^3 and matrix

Author Manuscript Author Manuscript Author Manuscript Author Manuscript

= 320 × 240 × 5. Images were obtained for different numbers of signal averages to vary SNR. Data were fit to monoexponential, stretched exponential and biexponential functions using the six methods investigated. Relative error maps were then calculated as described above in the *"Bias and Dispersion Calculations"* section. Parameter values obtained at the highest SNR were used as starting values for the NLLS-based methods.

RESULTS

Numerical Simulation Studies

Results of the MC simulations were obtained after removal of VEO. The number of removed VEO was almost identical among the six methods, and was less than 1% at the larger, though still moderate, SNR for each. Even at the lower SNR, corresponding to truly modest image quality, VEO represented only a relatively small fraction of the total voxels. Less than 2% of the voxels were excluded for the monoexponential, less than 5% for the stretched exponential, and less than 8% for the biexponential.

Fig. 2 shows the relative bias, as a measure of accuracy, and the relative dispersion, as a measure of precision, in parameter estimates for the monoexponential, with T_2 as the fit parameter of interest (Fig. 2a), the stretched exponential, with T_2 and α as fit parameters of interest (Fig. 2b) and the biexponential, with $T_{2,s}$, $T_{2,l}$, and f_s as fit parameters of interest (Fig. 2c). For the monoexponential signal model, all six methods showed bias and dispersion less than 10% in the estimation of T_2 for SNR > 30 (Fig. 2a). However, bias and dispersion increased rapidly with decreasing SNR, particularly with $NLLS_G$, $NLLS_{G,O}$, MAP_G and $MAP_{G,O}$. At SNR = 10, $NLLS_{\mathbf{R}}$ and $MAP_{\mathbf{R}}$ showed bias and dispersion less than 10%. Although $NLLS_{G,O}$ and $MAP_{G,O}$ were the most precise, showing the smallest dispersion, they were the least accurate, that is, showed the greatest bias, over the entire range of SNR. Overall, all methods showed comparable dispersion, but the methods using the proper noise model, $NLLS_{\mathbf{R}}$ and $MAP_{\mathbf{R}}$, demonstrated substantially lower bias. It is also of note that the Bayesian analysis always performed equivalently to or better than the corresponding NLLS analysis.

Results for the stretched exponential signal model are shown in Fig. 2b. For SNR > 20 all six methods showed a bias and dispersion of less than 15% in the estimation of T_2. Achieving these bounds for estimation of α required SNR > 30 for $NLLS_G$ and $NLLS_{G,O}$. Even at lower SNR's, $NLLS_{\mathbf{R}}$ and $MAP_{\mathbf{R}}$ remained highly accurate, that is, nearly bias-free, while bias became substantial for all other analyses. In addition, Fig. 2b shows that at the lower values of SNR, the dispersion in the estimates of T_2 and α obtained using the NLLS-based analyses was substantially higher than that obtained using the corresponding Bayesian-based methods.

Analysis of the biexponential signal model (Fig. 2c) indicates that bias becomes negligible as SNR increases for $NLLS_G$, $NLLS_{\mathbf{R}}$, MAP_G and $MAP_{\mathbf{R}}$ in the estimation of all parameters. In contrast, dispersion remains substantial, particularly for f_s and $T_{2,s}$. In general, at lower SNR's, $MAP_{\mathbf{R}}$ was found to provide the least biased parameter estimates. Similar performance was obtained using $NLLS_{\mathbf{R}}$ for the estimation of $T_{2,s}$ and $T_{2,l}$. In addition, the dispersion in parameters estimated using NLLS-based methods was

Author Manuscript Author Manuscript Author Manuscript Author Manuscript

substantially higher than that obtained using Bayesian-based methods. Finally, bias and dispersion for $T_{2,l}$ were substantially lower than for $T_{2,s}$, presumably due to the greater SNR and superior signal sampling for that component of the combined signal. $\mathrm{NLLS}_{\mathrm{G,O}}$ was found to perform well for $T_{2,l}$ estimation even at low SNR.

Figures 3-5 show relative bias and dispersion in the estimation of parameters for the monoexponential (Fig. 3), stretched exponential (Fig. 4) and biexponential (Fig. 5) signal models, for a range of underlying parameters and for two representative SNR's. Figure 3 shows that at high SNR, all methods performed well, with low bias and dispersion in the estimation of T_2. Differences in performance become apparent at lower SNR, for which the inclusion of the Rician noise model is of greater potential importance. We found that $\mathrm{NLLS}_{\mathbf{R}}$ and $\mathrm{MAP}_{\mathbf{R}}$ provided estimates with the least bias, that is, the greatest accuracy, while $\mathrm{MAP}_{\mathrm{G,O}}$ and $\mathrm{MAP}_{\mathbf{R}}$ provided estimates with the least dispersion, that is, the greatest precision, although $\mathrm{NLLS}_{\mathbf{R}}$ also provided precise estimates in several cases. Both bias and dispersion were found to decrease with increasing T_2, reflecting the higher SNR throughout the duration of the simulated data acquisition. Results for the stretched exponential signal model are shown in Fig. 4. At high SNR, all investigated methods provide low bias and dispersion in parameter estimation for the combinations of T_2 and α shown. However, at low SNR, $\mathrm{MAP}_{\mathbf{R}}$ was the least biased for the estimation of both T_2 and α, with $\mathrm{NLLS}_{\mathbf{R}}$ also performing well. This highlights the importance of appropriate noise modeling, regardless of the analytic method used for parameter estimation. Overall, the NLLS-based methods showed higher dispersion than the Bayesian-based methods. The bias and dispersion in estimates of T_2 and α decrease with increasing T_2, again reflecting improved SNR and signal sampling throughout the signal decay. Figure 5 summarizes the results for the biexponential signal model. As shown, the bias and dispersion in the estimation of f_s, $T_{2,s}$ and $T_{2,l}$ increase with a decreasing ratio $T_{2,l}/T_{2,s}$ or with increasing disparity between component sizes. In general, for low SNR, $\mathrm{MAP}_{\mathbf{R}}$ was found to be the least biased for the estimation of f_s, $T_{2,s}$ and $T_{2,l}$, with $\mathrm{NLLS}_{\mathbf{R}}$ also performing well in estimating $T_{2,s}$ and $T_{2,l}$. Overall, Fig. 5 indicates that the dispersion in the estimation of f_s, $T_{2,s}$ and $T_{2,l}$ obtained using the NLLS-based methods was higher than with the Bayesian-based methods.

Phantom Studies

As for the MC simulations, results of the phantom measurements were obtained after removal of VEO. Figure 6 shows the relative bias and dispersion, as a function of SNR, in parameter estimates determined from phantom measurements using single-phantom monoexponential (Fig 6a) and dual-phantom biexponential (Fig. 6b) data. At high SNR, all methods demonstrated low bias and dispersion. For the monoexponential case, at low to moderate SNR, the bias was substantially lower with $\mathrm{NLLS}_{\mathbf{R}}$ and $\mathrm{MAP}_{\mathbf{R}}$ than it was using the other methods for the estimation of T_2 (Fig. 6a). The dispersion in the estimation of T_2 was comparable among all methods. Similarly, for the biexponential analysis, bias in the estimates of $T_{2,s}$ and $T_{2,l}$ was minimized through use of $\mathrm{NLLS}_{\mathbf{R}}$ and $\mathrm{MAP}_{\mathbf{R}}$ (Fig. 6b). For f_s, $\mathrm{MAP}_{\mathbf{R}}$ was found to demonstrate the least bias, although all of the Bayesian-based methods performed well with the exception of $\mathrm{MAP}_{\mathrm{G,O}}$ in the estimation of $T_{2,l}$. This is likely attributable to the limited echo acquisition window, resulting in incomplete sampling of the decay of the $T_{2,l}$ component. This effect is also seen in the poor performance of $\mathrm{NLLS}_{\mathrm{G,O}}$.

Author Manuscript Author Manuscript Author Manuscript Author Manuscript

In addition, the dispersion in estimates of all derived parameters obtained using the NLLS-based methods was substantially greater as compared to Bayesian-based estimates.

The effect of the underlying parameters T_2, f_s, $T_{2,s}$and $T_{2,l}$ on the relative bias and dispersion in parameter estimates is summarized in Figs. 7-8. As shown, bias resulting from $\mathrm{NLLS}_{\mathbf{R}}$ and $\mathrm{MAP}_{\mathbf{R}}$ was the lowest, while dispersion using Bayesian-based methods was overall lower than using NLLS-based methods. In general, both bias and dispersion decreased with increasing T_2 (Fig. 7). For the biexponential case, bias and dispersion both increase with a decreasing ratio $T_{2,l}/T_{2,s}$ and with an increasing disparity between component sizes (Fig. 8).

In vivo Study

Figure 9 shows parameter maps derived from high SNR (~ 200) data (left hand column) using the six investigated methods, and corresponding parameter maps obtained at moderate SNR (~ 50), for monoexponential (Fig. 9a), stretched exponential (Fig. 9b) and biexponential (Fig. 9c) signal models. Figure 9 shows substantial random variation of estimated values in several image regions. To examine this in more detail, relative error maps, calculated as described in the Methods and describing the deviation of estimated parameter values from those obtained from the high SNR fiducial images, were created (Fig. 10). The mean and standard deviation of the relative errors are reported at the bottom of each error map. At the moderate SNR, all methods performed well for the estimation of T_2 in monoexponential decay, although $\mathrm{MAP}_{\mathbf{R}}$ and $\mathrm{NLLS}_{\mathbf{R}}$ were the best. These two methods also showed the best performance for the estimation of T_2 and α in the stretched exponential signal model. For biexponential analysis, the SNR was insufficient to provide a high-quality estimate of f_s using any of the analysis approaches, although $\mathrm{MAP}_{\mathbf{R}}$ performed the best. $T_{2,s}$ and $T_{2,l}$ were estimated more accurately, although only $T_{2,l}$ could be estimated to within ~ 15%, as achieved by $\mathrm{MAP}_{\mathbf{R}}$.

DISCUSSION

Parameter Estimation Methods

Bayesian Probability vs NLLS Approaches—The elegant work of Neil and Bretthorst (17) evaluated estimates of diffusion parameters for a two-compartment model at two values of SNR, using both simulations and spectroscopic NMR data exhibiting Gaussian noise. Substantial advantages were found for Bayesian analysis as compared to NLLS in terms of both accuracy and precision. Our work builds on this and extends it in several ways, using simulations, and phantom and human brain imaging experiments. First, we evaluate three distinct and widely-used signal models for transverse decay, the monoexponential, stretched exponential and biexponential. In addition, for each of these models, we evaluate the performance of three approaches to incorporating noise, namely, the assumption of Gaussian noise, the assumption of Gaussian noise that asymptotes to a non-zero value, and the assumption of Rician noise, as is most appropriate for magnitude MR images. Further, we evaluated the accuracy and precision with which parameters of interest can be estimated for wide ranges of SNR and underlying parameters.

Author Manuscript Author Manuscript Author Manuscript Author Manuscript

Overall, we found improved accuracy and precision using the Bayesian-based methods as compared to the NLLS-based methods (Figs. 2-8). This may be attributable to the fact that in Bayesian analysis, a given parameter is estimated independently of the others through marginalization, serving to reduce interdependence of parameter estimates by integrating over all values of the marginal parameters. This is in contrast to NLLS where unknown parameter estimates are highly correlated through the use of simultaneous estimation. This correlation has been previously demonstrated through Cramer-Rao lower bound calculations, MC simulations, and phantom measurements (8, 15-16). In addition, the NLLS algorithm may fail to find global minima due to the presence of local minima. Although such local minima are absent for the monoexponential, they are present for the bi- and stretched-exponential cases. This problem becomes more acute with the flattening of the surface of the least squares residuals seen with increasing model complexity (Supporting Figure S1). In fact, the performance of the Bayesian and NLLS methods were very similar for the monoexponential analysis, with the small differences being potentially attributable to the marginalization over A_0.

Finally, we found that in spite of its additional model complexity, potentially leading to substantial analytic difficulties, the performance of $\mathrm{MAP}_{\mathbf{R}}$ provides notable improvement in accuracy and precision compared to $\mathrm{NLLS}_{\mathbf{R}}$.

Rician vs Gaussian noise models—Our analyses show substantial improvements in accuracy and precision when Rician noise model is incorporated into the analysis of magnitude imaging data, with estimates performed through either NLLS or Bayesian analyses. Similar results have been previously reported for the estimation of T_1, T_2 and T_2^* using NLLS (12-13, 15), and for the estimation of T_2 using Bayesian analysis (21).

It is common practice to assume Gaussian-distributed noise in conventional magnitude MR images with high SNR (42, 63-66). Our results (Figs. 2-8) serve to validate this and demonstrate that high-quality parameter estimates may be obtained with the Gaussian approximation. However, we found that with more modest SNR, there is a substantial loss of performance. Attempting to compensate for the asymptotic positivity of the noise by using Gaussian noise with offset model was found to be of benefit when fitting data with small T_2, for which the signal is dominated by noise in the later echoes.

Unknown vs estimated noise parameters—All calculations were performed assuming known values for σ, σ^2 and, ε, such as would be based on separate measurements in order to reduce the dimensionality of parameter space. As expected, MC simulations (*data not shown*) indicate that this strategy resulted in increased accuracy, presumably through reducing the number of local minima and the interdependence of parameter estimates. A modest increase in precision was also found. In addition, computational times were considerably reduced, particularly for the Bayesian-based methods since marginalization over σ was not needed.

The quality of parameter estimates of course depends upon the quality of the estimates of $\hat{\sigma}, \hat{\alpha}^2 \quad and \quad \hat{\epsilon}$. Simulation analysis (Supporting Table S1) indicates that, as expected, moderate errors in the estimation of noise parameters, such as would be the case for

Author Manuscript Author Manuscript Author Manuscript Author Manuscript

estimation from large background regions of the image, have a negligible impact on parameter estimates. This was found to be the case for all fitting methods and for all three signal models. Clearly, the presence of non-random artifacts such as streaking or ghosting requires more sophisticated estimates of noise (67-68). In any event, in actual application, the strategy of independent noise estimation is to be preferred over incorporation of yet another parameter into the Bayesian or NLLS analysis.

Results of NLLS and Bayesian Probability Approaches

Performance of the NLLS-based methods—All three NLLS-based methods were found to be sensitive to initial estimates, highlighting the necessity of establishing a reproducible algorithm for selection of these estimates, especially in the low SNR regime. In contrast, at high SNR, convergence to global minima was attained even for relatively poor initial estimates (*data not shown*). However, in spite using true parameter values as starting points, we found a loss of performance as the total number of unknown parameters increased, such as in comparing the monoexponential to the biexponential. This is likely attributable to the increase in the number of local minima and to the flattening of the surface of least squares residuals as the number of parameters increases (Supporting Figure S1).

In some cases, we found that $\mathrm{NLLS}_{\mathbf{R}}$ compared favorably to $\mathrm{MAP}_{\mathbf{R}}$. However, our approach implemented an unrealistically favorable $\mathrm{NLLS}_{\mathbf{R}}$ analysis by providing true values as starting parameters, while in actual experiments these values are of course not known. It is well-known that inaccurate initial guesses render the NLLS algorithm highly susceptible to finding local rather than global minima (69), so that this procedure in effect penalizes the Bayesian analysis as compared to NLLS.

Performance of the Bayesian-based methods—One drawback of the Bayesian approaches is the computational time required to compute the integrals needed for the marginalization. In our direct implementation, computational time increased considerably with increasing dimensionality of the parameter space. To address this, the Markov Chain Monte Carlo method can be used so that the posterior distribution can be sampled, rather than directly computed (20, 70).

Numerical Simulations, Phantom and In vivo Studies

Our simulation results show that in the limit of high SNR, all six investigated methods yielded results that were accurate and precise. However, large differences in performance were seen at low to moderate SNR. Overall, $\mathrm{MAP}_{\mathbf{R}}$ performed the best of all methods, although $\mathrm{NLLS}_{\mathbf{R}}$ provided comparable results in many cases. As an example, the accuracy and precision of the estimate of the fraction of the rapidly decaying component, f_s, in the biexponential model were greatly improved using $\mathrm{MAP}_{\mathbf{R}}$ as compared to the other methods, including $\mathrm{NLLS}_{\mathbf{R}}$. This is of particular importance, since f_s has been proposed as a biomarker of pathology in several biological tissues, including cartilage (1-2, 38-39), bone (51) and brain (3-7, 40).

Our *in vivo* brain study indicates that, as expected, any of the six methods works well at high SNR. However, $\mathrm{MAP}_{\mathbf{R}}$ provides the most robust parameter estimates, especially in the low

Author Manuscript Author Manuscript Author Manuscript Author Manuscript

SNR regime. This can be seen visually from the parameter maps (Fig. 9) and from the error maps (Fig. 10). In contrast to MC simulations and phantom experiments, for the *in vivo* analyses there was no underlying correct model for comparison, and both monoexponential and biexponential models have been used in the analyses of transverse relaxation data from brain. In diffusion studies of brain, mono-, bi- and stretched-exponentials have all been applied (14, 43, 46, 71-73).

We found that in general, methods incorporating Rician noise performed better than those using Gaussian noise, regardless of the signal model. This is in agreement with previous work on cartilage for monoexponential T_2 (12) and biexponential T_2^* (15) measurements. Our results also indicate that Bayesian-based methods exhibit higher precision than NLLS-based methods.

Our MC simulations, and phantom and *in vivo* experiments, all highlight the importance of considering the correct form of the noise distribution for magnitude MR images. We have used the Rician distribution, as is appropriate for single-coil signal reception. However, multiple receiver coils are widely used to increase speed or SNR. If uncorrelated, equally distributed and stationary noise is assumed, the noise distribution in the resulting magnitude images is described by a non-central χ-distributions

$$P_\chi\left(S_n|A\left(\theta;\mathbf{TE_n}\right),\sigma,R\right)=\frac{A\left(\theta;\mathbf{TE_n}\right)}{\sigma^2}\left(\frac{S_n}{A\left(\theta;\mathbf{TE_n}\right)}\right)^R exp\left(-\frac{A^2\left(\theta;\mathbf{TE_n}\right)+S_n^2}{2\sigma^2}\right)I_{R-1}\left(\frac{S_nA\left(\theta;\mathbf{TE_n}\right)}{\sigma^2}\right)$$

where R denotes the number of channels (55, 74). The corresponding likelihood function is given by

$$L_\chi\left(\mathbf{S}|\theta,\sigma\right)=\prod_{n=1}^{N}P_\chi\left(S_n|A\left(\theta;\mathbf{TE_n}\right),\sigma,R\right)$$

This expression can be incorporated into a Bayesian approach for parameter estimation in a fashion analogous to the above. This can be compared to an NLLS minimization using the first moment of $P_\chi(S_n \mid A(\theta;TE_n),\sigma,R)$ as the expectation value of the acquired data

$$E_\chi\left[S_n\right]=\frac{1\cdot3\cdot5\ldots(2R-1)}{2^{R-1}(R-1)!}\sqrt{\frac{\pi\sigma^2}{2}}\quad{}_1F_1\left(-\frac{1}{2},R,-\frac{A^2\left(\theta;\mathbf{TE_n}\right)}{2\sigma^2}\right)$$

(75-78), where ${}_1F_1$ is a confluent hypergeometric function.

Our results indicate that in general, Bayesian analysis provides more reliable estimates of transverse decay parameters than does NLLS when the underlying signal model is known. In realistic experiments, the correct signal model may be unknown. We believe that previous results (17, 20, 79) and the results presented here provide strong motivation for investigations of model selection using Bayesian probability theory.

Author Manuscript Author Manuscript Author Manuscript Author Manuscript

Supplementary Material

Refer to Web version on PubMed Central for supplementary material.

ACKNOWLEDGEMENTS

We gratefully acknowledge the anonymous reviewers for their helpful comments. This work was supported by the Intramural Research Program of the NIH, National Institute on Aging.

APPENDIX

We define details of the marginalization used in Bayesian parameter estimation. To obtain the estimated parameter, $\hat{\theta}_i$, (Eqs. A1-A6), the corresponding posterior probability, P(θ_i | **S**,σ), was computed for a grid of parameter values, θ_i. The MAP estimate, $\hat{\theta}_i$, corresponds to the value for which P(θ_i | **S**,σ) attains the maximum of the computed values (17, 20-21, 37). Integrals were performed numerically using the *integral*, *integral2* and *integral3* commands in Matlab for mono-, stretched-, and biexponential signal models, respectively. The integration limits were chosen such that the contribution of the relevant likelihood function to the integral outside these limits was negligible.

Bayesian inference requires assignment of a prior probability based on pre-existing knowledge (80). This choice becomes of particular importance when the likelihood function is not the dominant term in the posterior probability such as is often the case when only a limited number of measurements are available (37). In the present work, the number of measurements was much greater than the number of derived parameters, so that results are largely independent of reasonable selections of prior probabilities (*data not shown*). We assumed a formally improper uniform prior in all cases; that is, the P(θ) term in Eq. 7 was taken as unity. With limited data, the selection of the prior is more critical (37).

Likelihood functions for Bayesian-based methods

Each Bayesian-based method is defined by its likelihood function, $L(\mathbf{S}|\theta,\sigma)$ and a uniform prior. For $MAP_{\mathbf{R}}$, $L(\mathbf{S}|\theta,\sigma) = L_{Rice}(\mathbf{S}|\theta,\sigma)$ (Eq. 3), for MAP_G , $L(\mathbf{S}|\theta,\sigma) = L_{Gauss}(\mathbf{S}|\theta,\sigma)$ (Eq. 6), and for $MAP_{G,O}$, $L(\mathbf{S}|\theta,\sigma) = L_{Gauss}(\mathbf{S}|\theta,\sigma)$ with $A(\theta;TE_n)$ in Eq. 6 replaced by $A(\theta;TE_n) + \varepsilon$.

Marginalization Integrals for Signal Models

Monoexponential Signal Model

The estimate of T_2 was obtained according to

$$\hat{T}_2 = \underset{T_2}{argmax}\left\{\mathrm{P}\left(T_2|\mathbf{S},\sigma\right)\right\} = \underset{T_2}{argmax}\left\{\int L\left(\mathbf{S}|\theta,\sigma\right)dA_0\right\} \quad \text{[A.1]}$$

where $A(\theta;TE_n)$ is given by Eq. 10.

Author Manuscript Author Manuscript Author Manuscript Author Manuscript

Stretched Exponential Signal Model

Estimates of T_2 and α were obtained according to

$$\hat{T}_2 = \underset{T_2}{argmax}\left\{\mathrm{P}\left(T_2|\mathbf{S},\sigma\right)\right\} = \underset{T_2}{argmax}\left\{\int\int L\left(\mathbf{S}|\theta,\sigma\right)dA_0 d\alpha\right\} \quad [A.2]$$

$$\hat{\alpha} = \underset{\alpha}{argmax}\left\{\mathrm{P}\left(\alpha|\mathbf{S},\sigma\right)\right\} = \underset{\alpha}{argmax}\left\{\int\int L\left(\mathbf{S}|\theta,\sigma\right)dA_0 dT_2\right\} \quad [A.3]$$

where $A(\theta;TE_n)$ is given by Eq. 11.

Biexponential Signal Model

Estimates of f_s, $T_{2,s}$ and $T_{2,l}$ were obtained according to

$$\hat{f}_s = \underset{fs}{argmax}\left\{\mathrm{P}\left(f_s|\mathbf{S},\sigma\right)\right\} = \underset{fs}{argmax}\left\{\int\int\int L\left(\mathbf{S}|\theta,\sigma\right)dA_0 dT_{2,s} dT_{2,l}\right\} \quad [A.4]$$

$$\hat{T}_{2,s} = \underset{T_{2,s}}{argmax}\left\{\mathrm{P}\left(T_{2,s}|\mathbf{S},\sigma\right)\right\} = \underset{T_{2,s}}{argmax}\left\{\int\int\int L\left(\mathbf{S}|\theta,\sigma\right)dA_0 df_s dT_{2,l}\right\} \quad [A.5]$$

$$\hat{T}_{2,l} = \underset{T_{2,l}}{argmax}\left\{\mathrm{P}\left(T_{2,l}|\mathbf{S},\sigma\right)\right\} = \underset{T_{2,l}}{argmax}\left\{\int\int\int L\left(\mathbf{S}|\theta,\sigma\right)dA_0 df_s dT_{2,s}\right\} \quad [A.6]$$

where $A(\theta;TE_n)$ is given by Eq. 12.

REFERENCES

1. Reiter DA, Roque RA, Lin PC, Doty SB, Pleshko N, Spencer RG. Improved Specificity of Cartilage Matrix Evaluation using Multiexponential Transverse Relaxation Analysis Applied to Pathomimetically Degraded Cartilage. NMR Biomed. 2011; 24:1286–1294. [PubMed: 21465593]
2. Reiter DA, Lin PC, Fishbein KW, Spencer RG. Multicomponent T_2 Relaxation Analysis in Cartilage. Magn Reson Med. 2009; 61:803–809. [PubMed: 19189393]
3. MacKay A, Laule C, Vavasour I, Bjarnason T, Kolind S, Mädler B. Insights into Brain Microstructure from the T_2 Distribution. Magn Reson Imaging. 2006; 24:515–525. [PubMed: 16677958]
4. Webb S, Munro CA, Midha R, Stanisz GJ. Is Multicomponent T_2 a good Measure of Myelin Content in Peripheral Nerve? Magn Reson Med. 2003; 49:638–645. [PubMed: 12652534]
5. Kolind SH, Laule C, Vavasour IM, Li DK, Traboulsee AL, Mädler B, Moore GR, MacKay AL. Complementary Information from Multi-exponential T_2 Relaxation and Diffusion Tensor Imaging Reveals Differences between Multiple Sclerosis Lesions. Neuroimage. 2008; 40:77–85. [PubMed: 18226549]
6. Junyu, Guo; Qing, Ji; Wilburn, E. Reddick. Multi-slice Myelin Water Imaging for Practical Clinical Applications at 3.0 T. Magn Reson Med. 2013; 70:813–822.
7. Harkins KD, Valentine WM, Gochberg DF, Does MD. *In vivo* Multi-exponential T_2, Magnetization Transfer and Quantitative Histology in a Rat Model of Intramyelinic Edema. Neuroimage Clin. 2013; 2:810–817. [PubMed: 24179832]
8. Celik H, Bouhrara M, Reiter DA, Fishbein KW, Spencer RG. Stabilization of the Inverse Laplace Transform of Multiexponential Decay through Introduction of a Second Dimension. J Magn Reson. 2013; 236:134–139. [PubMed: 24035004]

Author Manuscript Author Manuscript Author Manuscript Author Manuscript

9. Day IJ. On the Inversion of Diffusion NMR Data: Tikhonov Regularization and Optimal Choice of the Regularization Parameter. J Magn Reson. 2011; 211:178–185. [PubMed: 21683632]
10. Rice, SO. Mathematical analysis of random noise. In: Wax, N., editor. Selected papers on noise and stochastic processes. Dover Publications Inc.; New York, NY: 1954. p. 133-194.
11. Bernstein MA, Thomasson DM, Perman WH. Improved Detectability in Low Signal-to-Noise Ratio Magnetic Resonance Images by Means of Phase-corrected Real Reconstruction. Med Phys. 1989; 16:813–817. [PubMed: 2811764]
12. Raya JG, Dietrich O, Horng A, Weber J, Reiser MF, Glaser C. T_2 Measurement in Articular Cartilage: Impact of the Fitting Method on Accuracy and Precision at Low SNR. Magn Reson Med. 2010; 63:181–193. [PubMed: 19859960]
13. Karlsen OT, Verhagen R, Bovée WMMJ. Parameter Estimation From Rician-Distributed Data Sets Using a Maximum Likelihood Estimator: Application to T_1 and Perfusion Measurements. Magn Reson Med. 1999; 41:614–623. [PubMed: 10204887]
14. Kristoffersen A. Estimating Non-Gaussian Diffusion Model Parameters in the Presence of Physiological Noise and Rician Signal Bias. J Magn Reson Imaging. 2012; 35:181–189. [PubMed: 21972173]
15. Bouhrara M, Reiter DA, Celik H, Bonny JM, Lukas V, Fishbein KW, Spencer GS. Incorporation of Rician Noise in the Analysis of Biexponential Transverse Relaxation in Cartilage using a Multiple Gradient Echo Sequence at 3 and 7 Tesla. Magn Reson Med. 2014 DOI: 10.1002/mrm.25111.
16. Anastasiou A, Hall LD. Optimization of T_2 and M_0 Measurements of Biexponential Systems. Magn Reson Imaging. 2004; 22:67–80. [PubMed: 14972396]
17. Neil JJ, Bretthorst GL. On the use of Bayesian Probability Theory for Analysis of Exponential Decay Data: an Example Taken from Intravoxel Incoherent Motion Experiments. Magn Reson Med. 1993; 29:642–647. [PubMed: 8505900]
18. Orton MR, Collins DJ, Walker-Samuel S, d'Arcy JA, Hawkes DJ, Atkinson D, Leach MO. Bayesian Estimation of Pharmacokinetic Parameters for DCE-MRI with a Robust Treatment of Enhancement Onset Time. Phys Med Biol. 2007; 52:2393–2408. [PubMed: 17440242]
19. Transtrum MK, Machta BB, Sethna JP. Why are nonlinear fits to data so challenging? Phys Rev Lett. 2010; 104:060201. [PubMed: 20366807]
20. Bretthorst GL, Hutton WC, Garbow JR, Ackerman JJH. Exponential Parameter Estimation (in NMR) Using Bayesian Probability Theory. Concepts in Magn Reson. 2005; 27A:55–63.
21. Walker-Samuel S, Orton M, McPhail LD, Boult JK, Box G, Eccles SA, Robinson SP. Bayesian Estimation of Changes in Transverse Relaxation Rates. Magn Reson Med. 2010; 64:914–921. [PubMed: 20806382]
22. Papoulis, A. Probability, random variables and stochastic processes. second. McGraw-Hill; Tokyo: 1984.
23. Sijbers J, den Dekker AJ, Verhoye M, Van Audekerke J, Van Dyck D. Estimation of Noise from Magnitude MR Images. Magn Reson Imaging. 1998; 16:87–90. [PubMed: 9436952]
24. Lehmann, EL.; Casella, G. Theory of Point Estimation. second. Springer-Verlag; New York. 1998.
25. Gudbjartsson H, Patz S. The Rician Distribution of Noisy MRI Data. Magn Reson Med. 1995; 34:910–914. [PubMed: 8598820]
26. Kroenke CD, Bretthorst GL, Inder TE, Neil JJ. Modeling Water Diffusion Anisotropy Within Fixed Newborn Primate Brain Using Bayesian Probability Theory. Magn Reson Med. 2006; 55:187–197. [PubMed: 16342153]
27. Bretthorst, GL. Lecture Notes in Statistics. Vol. 48. Springer-Verlag; New York: 1988. Bayesian Spectrum Analysis and Parameter Estimation.
28. Bretthorst GL. Bayesian Analysis I. Parameter Estimation Using Quadrature NMR Models. J Magn Reson. 1990; 88:533–551.
29. Xing D, Gibbs SJ, Derbyshire JA, Fordham EJ, Carpenter TA, Hall LD. Bayesian Analysis for Quantitative NMR Flow and Diffusion Imaging. J Magn Reson. 1995; 106:1–9.
30. Quirk JD, Sukstanskii AL, Bretthorst GL, Yablonskiy DA. Optimal Decay Rate Constant Estimates from Phased Array Data utilizing Joint Bayesian Analysis. J Magn Reson. 2009; 198:49–56. [PubMed: 19181549]

Author Manuscript Author Manuscript Author Manuscript Author Manuscript

31. Üstündağ D, Cevri M. Recovering Sinusoids from Noisy Data using Bayesian Inference with Simulated Annealing. Math Comput Appli. 2011; 16:382–391.
32. Payne SJ. A Bayesian Approach for the Estimation of Model Parameters from Noisy Data Sets. IEEE Signal Proc Letters. 2005; 12:553–556.
33. Jbabdi S, Woolrich MW, Andersson JL, Behrens TE. A Bayesian Framework for Global Tractography. NeuroImage. 2007; 37:116–129. [PubMed: 17543543]
34. Jbabdi S, Sotiropoulos SN, Savio AM, Graña M, Behrens TE. Model-based Analysis of Multishell Diffusion MR Data for Tractography: How to get over Fitting Problems. Magn Reson Med. 2012; 68:1846–1855. [PubMed: 22334356]
35. Bayes T. An Essay towards solving a Problem in the Doctrine of Chances. Philosophical Transactions of the Royal Society of London. 1763; 53:370–418.
36. Laplace P. Mémoire sur la Probabilité des Causes par les Evènements. l'Académie Royale des Sciences. 1774; 61:621–656. 359–378. English translation by S.M. Stigler in 1986 as "Memoir on the Probability of the Causes of Events" in Statistical Science.
37. Murphy, KP. Machine Learning: a Probabilistic Perspective. The MIT Press; 2012.
38. Reiter DA, Roque RA, Lin PC, Irrechukwu O, Doty S, Longo DL, Pleshko N, Spencer RG. Mapping Proteoglycan-Bound Water in Cartilage: Improved Specificity of Matrix Assessment using Multiexponential Transverse Relaxation Analysis. Magn Reson Med. 2011; 65:377–384. [PubMed: 21264931]
39. Xia Y, Moody JB, Alhadlaq H. Orientational Dependence of T_2 relaxation in Articular Cartilage: a Microscopic MRI (micro MRI) Study. Magn Reson in Med. 2002; 48:460–469. [PubMed: 12210910]
40. Meyers SM, Laule C, Vavasour IM, Kolind SH, Mädler B, Tam R, Traboulsee AL, Lee J, Li DK, MacKay AL. Reproducibility of Myelin Water Fraction Analysis: a Comparison of Region of Interest and Voxel-based Analysis Methods. Magn Reson Imaging. 2009; 27:1096–1103. [PubMed: 19356875]
41. Deoni SC, Matthews L, Kolind SH. One Component? Two Components? Three? The Effect of Including a Nonexchanging "Free" Water Component in Multicomponent Driven Equilibrium Single Pulse Observation of T_1 and T_2. Magn Reson Med. 2013; 70:147–154. [PubMed: 22915316]
42. Whittall KP, MacKay AL, Li DK. Are Mono-exponential Fits to a Few Echoes Sufficient to Determine T_2 Relaxation for *In vivo* Human Brain? Magn Reson Med. 1999; 41:1255–1257. [PubMed: 10371459]
43. Kristoffersen A. Optimized Quantification of Diffusional Non-Gaussianity in the Human Brain. J Magn Reson Imaging. 2013; 38:1434–1444. [PubMed: 23559256]
44. Hall MG, Barrick TR. From Diffusion-Weighted MRI to Anomalous Diffusion Imaging. Magn Reson Med. 2008; 59:447–455. [PubMed: 18224695]
45. Palombo M, Gabrielli A, De Santis S, Capuani S. The γ Parameter of the Stretched-exponential Model is Influenced by Internal Gradients: Validation in Phantoms. J Magn Reson. 2012; 216:28–36. [PubMed: 22277782]
46. Ingo C, Magin RL, Colon-Perez L, Triplett W, Mareci TH. On random Walks and Entropy in Diffusion-weighted Magnetic Resonance Imaging Studies of Neural Tissue. Magn Reson Med. 2013; 71:617–627. [PubMed: 23508765]
47. Magin RL, Li W, Pilar Velasco M, Trujillo J, Reiter DA, Morgenstern A, Spencer RG. Anomalous NMR Relaxation in Cartilage Matrix Components and Native Cartilage: Fractional-order Models. J Magn Reson. 2011; 210:184–191. [PubMed: 21498095]
48. Lattanzio PJ, Marshall KW, Damyanovich AZ, Peemoeller H. Macromolecule and Water Magnetization Exchange Modeling in Articular Cartilage. Magn Reson Med. 2000; 44:840–851. [PubMed: 11108620]
49. Ababneh Z, Beloeil H, Berde CB, Gambarota G, Maier SE, Mulkern RV. Biexponential Parameterization of Diffusion and T_2 Relaxation Decay Curves in a Rat Muscle Edema Model: Decay Curve Components and Water Compartments. Magn Reson Med. 2005; 54:524–531. [PubMed: 16086363]

Author Manuscript Author Manuscript Author Manuscript Author Manuscript

50. Diaz E, Chung CB, Bae WC, Statum S, Znamirowski R, Bydder GM, Du J. Ultrashort Echo Time Spectroscopic Imaging (UTESI): an Efficient Method for Quantifying Bound and Free Water. NMR Biomed. 2012; 25:161–168. [PubMed: 21766381]
51. Du J, Bydder GM. Qualitative and Quantitative Ultrashort-TE MRI of Cortical Bone. NMR Biomed. 2013; 26:489–506. [PubMed: 23280581]
52. He T, Gatehouse PD, Smith GC, Mohiaddin RH, Pennell DJ, Firmin DN. Myocardial T_2^* Measurements in Iron-overloaded Thalassemia: an *In vivo* Study to Investigate Optimal Methods of Quantification. Magn Reson Med. 2008; 60:1082–1089. [PubMed: 18956471]
53. Juras V, Apprich S, Zbýň S, Zak L, Deligianni X, Szomolanyi P, Bieri O, Trattnig S. Quantitative MRI Analysis of Menisci Using Biexponential T_2^* Fitting with a Variable Echo Time Sequence. Magn Reson Med. 2014; 71:1015–1023. [PubMed: 23606167]
54. Ghugre NR, Enriquez CM, Coates TD, Nelson MD, Wood JC. Improved R_2^* Measurements in Myocardial Iron Overload. J Magn Reson Imaging. 2006; 23:9–16. [PubMed: 16329085]
55. Edelstein WA, Bottomley PA, Pfeifer LM. A Signal-to-Noise Calibration Procedure for NMR Imaging Systems. Med Phys. 1984; 11:180–185. [PubMed: 6727793]
56. Constantinides CD, Atalar E, McVeigh ER. Signal-to-Noise Measurements in Magnitude Images from NMR Phased Arrays. Magn Reson Med. 1997; 38:852–857. [PubMed: 9358462]
57. Aja-Fernández S, Alberola-López C, Westin CF. Noise and Signal Estimation in Magnitude MRI and Rician Distributed Images: A LMMSE Approach. IEEE Trans Image Process. 2008; 17:1383–1898. [PubMed: 18632347]
58. Sijbers J, den Dekker AJ. Maximum Likelihood Estimation of Signal Amplitude and Noise Variance From MR Data. Magn Reson Med. 2004; 51:586–594. [PubMed: 15004801]
59. Hoaglin, D.; Mosteller, F.; Tukey, J. Understanding Robust and Exploratory Data Analysis. John Wiley & Sons; New York: 1983.
60. McGibney G, Smith MR. An Unbiased Signal-to-Noise Ratio Measure for Magnetic Resonance Imaging. Med Phys. 1993; 20:1077–1078. [PubMed: 8413015]
61. Carr HY, Purcell EM. Effects of Diffusion on Free Precession in Nuclear Magnetic Resonance Experiments. Phys Rev. 1954; 94:630–637.
62. Meiboom S, Gill D. Modified Spin-echo Method for Measuring Nuclear Relaxation Times. Rev Sci Intrum. 1958; 29:688–691.
63. Bonny JM, Zanca M, Boire JY, Veyre A. T_2 Maximum Likelihood Estimation from Multiple Spin-echo Magnitude Images. Magn Reson Med. 1996; 36:287–296. [PubMed: 8843383]
64. Shrager RI, Weiss GH, Spencer RG. Optimal Sampling Strategies for T_2 Measurements: Monoexponential and Biexponential Systems. NMR Biomed. 1998; 11:297–305. [PubMed: 9802472]
65. Jones DK, Basser PJ. "Squashing Peanuts and Smashing Pumpkins": How Noise Distorts Diffusion-weighted MR Data. Magn Reson Med. 2004; 52:979–993. [PubMed: 15508154]
66. Jones JA, Hodgkinson P, Barker AL, Hore PJ. Optimal Sampling Strategies for the Measurement of spin-spin Relaxation Times. J Magn Reson. 1996; 113:25–34.
67. Coupé P, Manjón JV, Gedamu E, Arnold D, Robles M, Collins DL. Robust Rician Noise Estimation for MR Images. Med Image Anal. 2010; 14:483–493. [PubMed: 20417148]
68. Rajan, J.; Poot, D.; Juntu, J.; Sijbers, J. Segmentation Based Noise Variance Estimation from Background MRI Data. Proceedings of the 7th International Conference on Image Analysis and Recognition; Springer-Verlag. 2010. p. 62-70.
69. Press, WH.; Teukolsky, SA.; Vetterling, WT.; Flannery, BP. The Art of Scientific Computing. Cambridge University Press; Cambridge, UK: 1992. Numerical recipes in C.
70. Metropolis N, Ulam S. The Monte Carlo method. J Amer Statist Assoc. 1949; 44:335–341.
71. Bennett KM, Schmainda KM, Bennett RT, Rowe DB, Lu H, Hyde JS. Characterization of Continuously Distributed Cortical Water Diffusion Rates with a Stretched-exponential Model. Magn Reson Med. 2003; 50:727–734. [PubMed: 14523958]
72. Grinberg F, Farrher E, Ciobanu L, Geffroy F, Le Bihan D, Shah NJ. Non-Gaussian Diffusion Imaging for Enhanced Contrast of Brain Tissue Affected by Ischemic Stroke. PloS One. 2014; 27:e89225. 9(2). [PubMed: 24586610]

Author Manuscript Author Manuscript Author Manuscript Author Manuscript

73. Mulkern RV, Haker SJ, Maier SE. On High b Diffusion Imaging in the Human Brain: Ruminations and Experimental Insights. Magn Reson Med. 2009; 27:1151–1162.
74. Miller, KS. Multidimensional Gaussian Distributions. John Wiley and Sons Inc.; New York: 1964. p. 26-42.
75. Koay CG, Basser PJ. Analytically Exact Correction Scheme for Signal Extraction from Noisy Magnitude MR Signals. J Magn Reson. 2006; 179:317–322. [PubMed: 16488635]
76. Wang C, He T, Liu X, Zhong S, Chen W, Feng Y. Rapid Look-up Table Method for Noise-corrected Curve Fitting in the R_2^* Mapping of Iron Loaded Liver. Magn Reson Med. 2014 DOI: 10.1002/mrm.25184.
77. Feng Y, He T, Gatehouse PD, Li X, Harith Alam M, Pennell DJ, Chen W, Firmin DN. Improved MRI R_2^* Relaxometry of Iron-loaded Liver with Noise Correction. Magn Reson Med. 2013; 70:1765–1774. [PubMed: 23359410]
78. Hardy PA, Andersen AH. Calculating T_2 in Images from a Phased Array Receiver. Magn Reson Med. 2009; 61:962–969. [PubMed: 19215046]
79. Bretthorst GL, Hutton WC, Garbow JR, Ackerman JJH. Exponential Model Selection (in NMR) using Bayesian Probability Theory. Concepts Magn Reson. 2005; 27A:64–72.
80. Jaynes ET. Prior Probabilities. IEEE Trans Syst Sci Cybern. 1968; 4:227–241.

Author Manuscript Author Manuscript Author Manuscript Author Manuscript

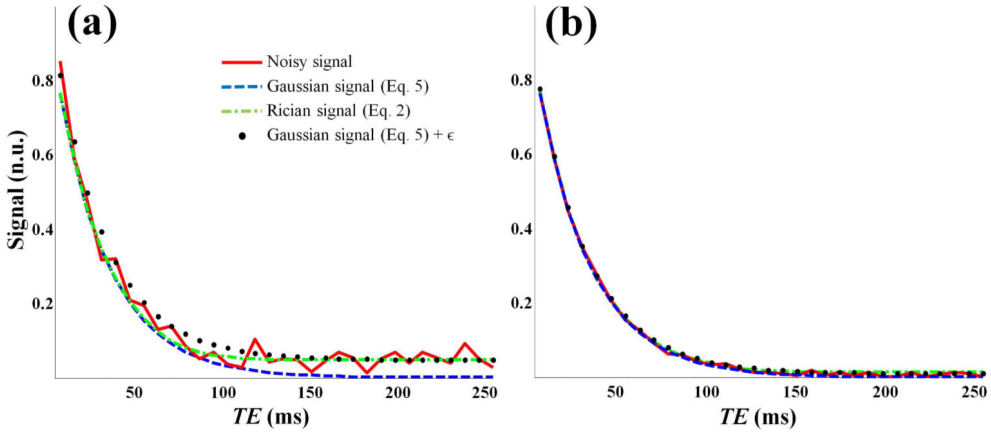

Fig. 1.

Signals as a function of TE_n generated for T_2 = 30 ms and A_0 = 1, assuming monoexponential transverse decay (Eq. 10) with SNR of 20 (Panel a) and 100 (Panel b). The noisy signal, $S(TE_n)$, was obtained through addition of Rician noise to the underlying noise-free signal, $A(\theta;TE_n)$, according to $S(TE_n) = \sqrt{(A(\theta;\mathbf{TE_n}) + N_{re})^2 + N_{im}^2}$ where the noise in the real and imaginary channels, N_{re} and N_{im}, was generated from a Gaussian distribution with zero mean and standard deviation σ.

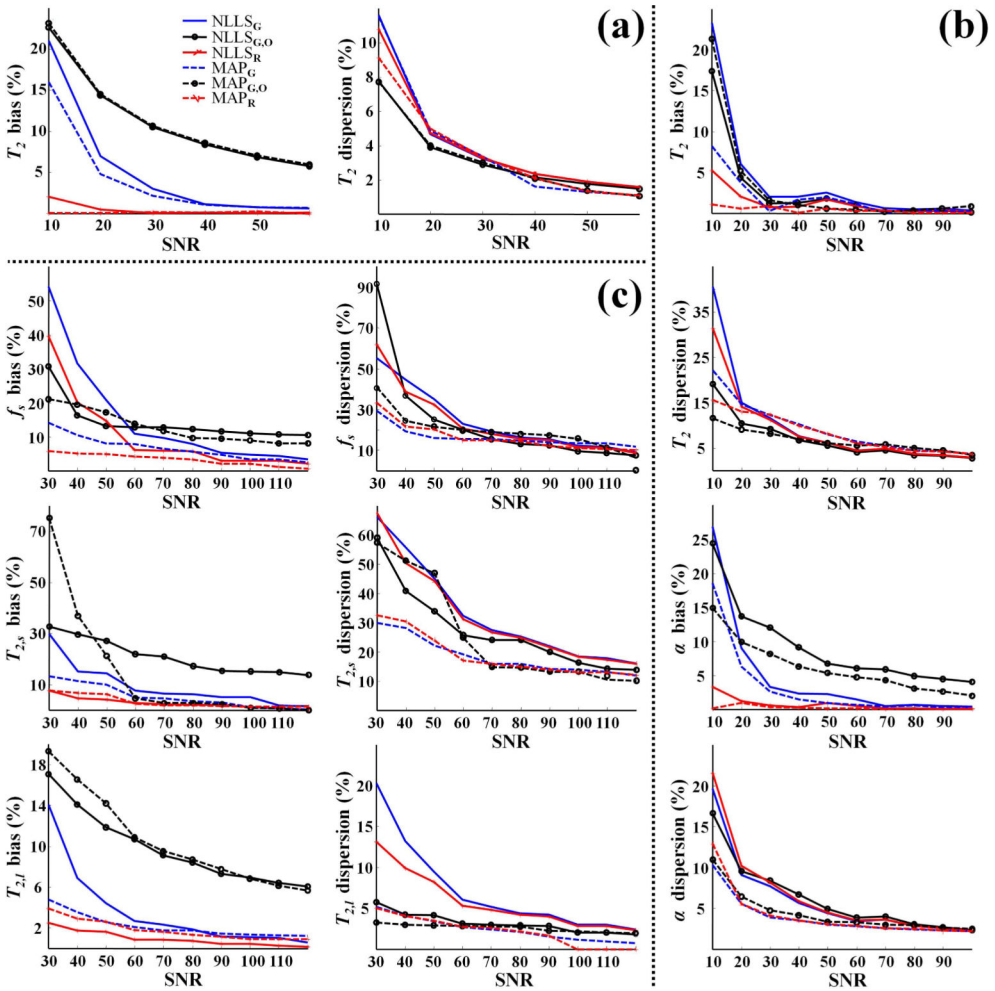

Fig. 2.

Monte Carlo simulation results for all three investigated signal models showing relative bias and dispersion in parameter estimates as a function of SNR using the fitting methods $NLLS_G$, $NLLS_{G,O}$, $NLLS_{\mathbf{R}}$, MAP_G, $MAP_{G,O}$ and $MAP_{\mathbf{R}}$. (a) Results for T_2 assuming the monoexponential signal model with T_2 = 70 ms as the underlying parameter value. (b) Results for T_2 and α assuming the stretched exponential signal model with T_2 = 60 ms and α = 0.8. (c) Results for f_s, $T_{2,s}$ and $T_{2,l}$ assuming the biexponential signal model with f_s = 0.25, $T_{2,s}$ = 20 ms and $T_{2,l}$ = 90 ms. Overall, bias and dispersion were substantially reduced through use of Rician noise model and Bayesian analysis; see text for detailed discussion.

Author Manuscript Author Manuscript Author Manuscript Author Manuscript

Author Manuscript Author Manuscript Author Manuscript Author Manuscript

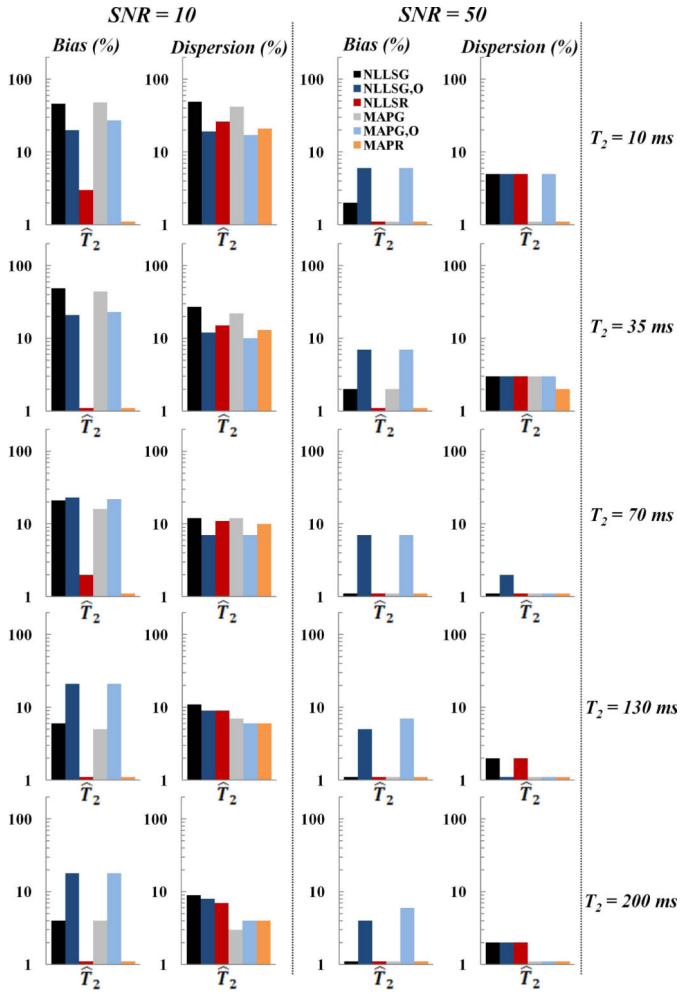

Fig. 3.

Relative bias and dispersion in T_2 estimates obtained using Monte Carlo simulations for the monoexponential signal model at SNR of 10 (left column) and 50 (middle column) using the $NLLS_G$, $NLLS_{G,O}$, $NLLS_{\mathbf{R}}$, MAP_G, $MAP_{G,O}$ and $MAP_{\mathbf{R}}$ analysis methods for five different input T_2 values (right column). Decreased bias and dispersion, that is, improved accuracy and precision, were achieved through use of Rician noise model and Bayesian analysis as discussed in detail in the text.

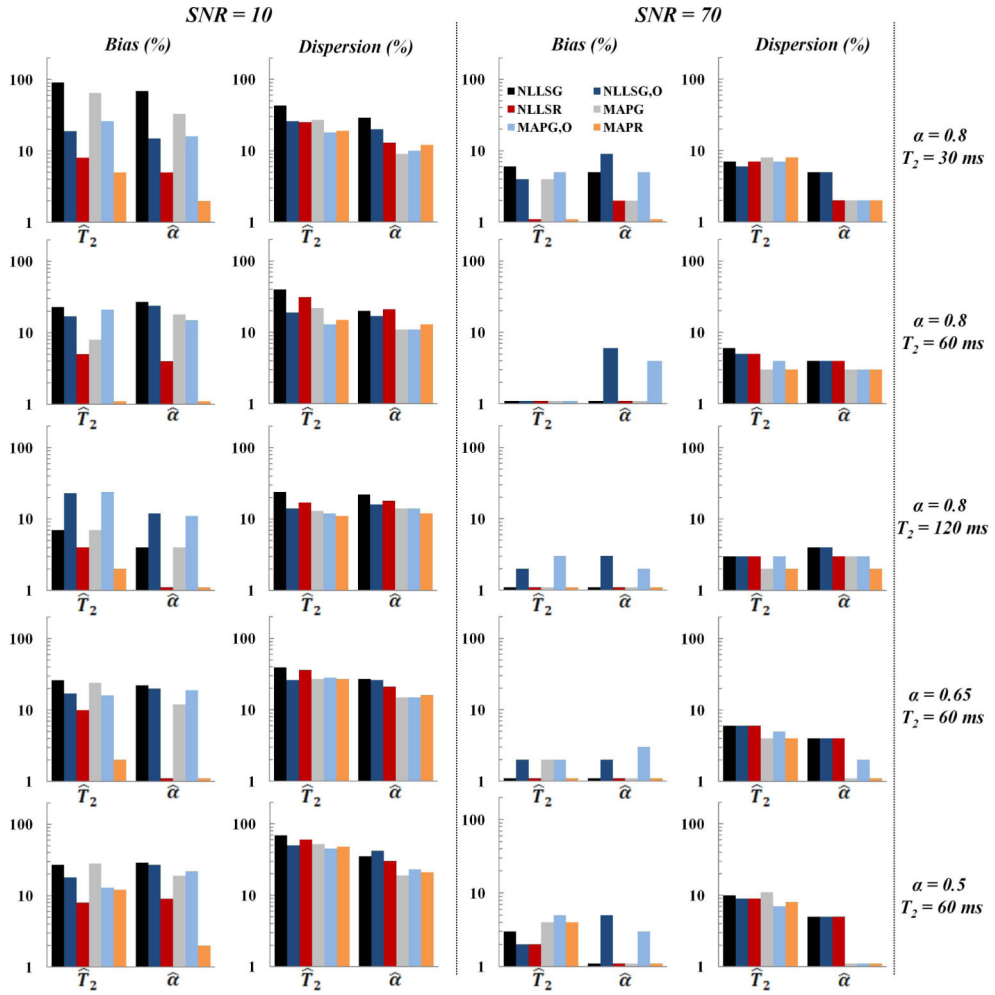

Fig. 4.

Relative bias and dispersion of T_2 and α estimates obtained using Monte Carlo simulations for the stretched exponential signal model at SNR 10 (left column) and 70 (middle column) using $NLLS_G$, $NLLS_{G,O}$, $NLLS_{\mathbf{R}}$, MAP_G, $MAP_{G,O}$ and $MAP_{\mathbf{R}}$ analysis methods for five different combinations of T_2 and α values (right column). Decreased bias and dispersion, that is, improved accuracy and precision, were achieved through use of Rician noise model and Bayesian analysis as discussed in detail in the text.

Author Manuscript Author Manuscript Author Manuscript Author Manuscript

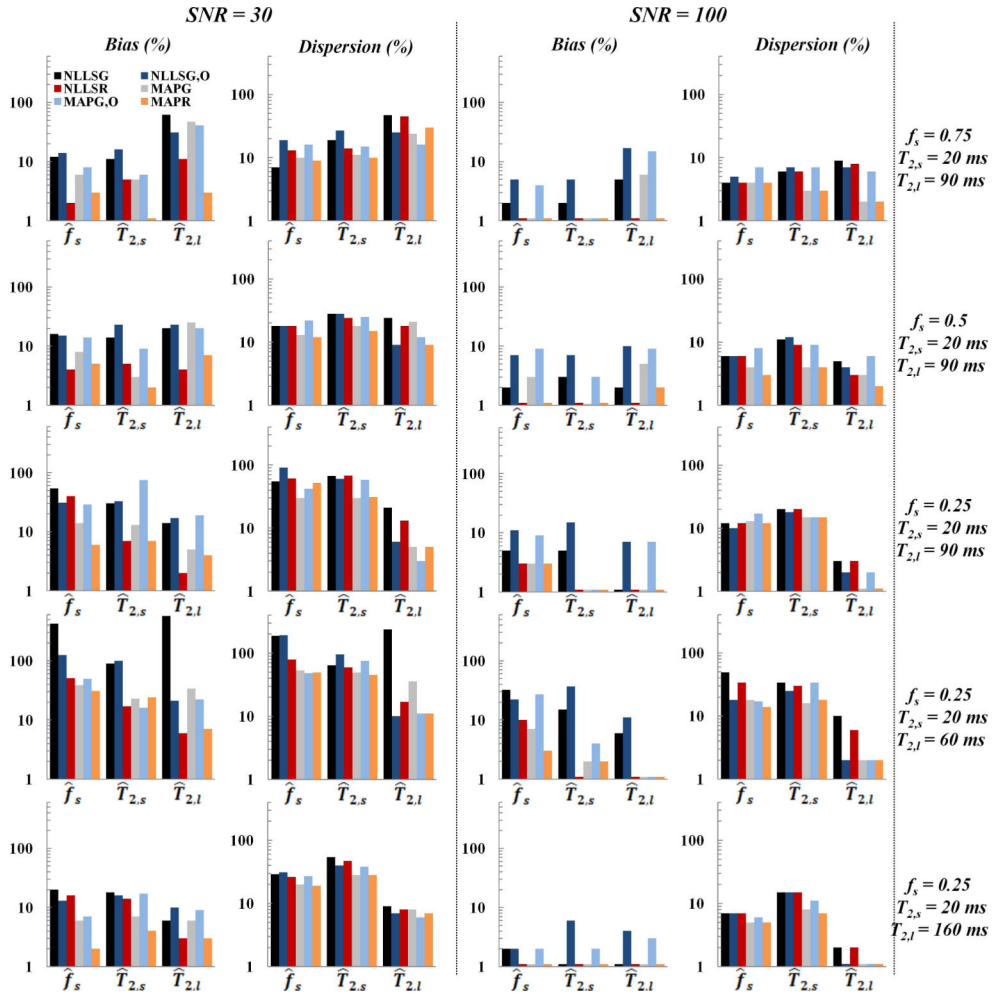

Fig. 5.

Relative bias and dispersion of the estimates of f_s, $T_{2,s}$ and $T_{2,l}$ obtained using Monte Carlo simulations for the biexponential signal model at SNR of 30 (left column) and 100 (middle column) using $\mathrm{NLLS_G}$, $\mathrm{NLLS_{G,O}}$, $\mathrm{NLLS_{\mathbf{R}}}$, $\mathrm{MAP_G}$, $\mathrm{MAP_{G,O}}$ and $\mathrm{MAP_{\mathbf{R}}}$ analysis methods for five different combinations of f_s, $T_{2,s}$ and $T_{2,l}$ (right column). Decreased bias and dispersion, that is, improved accuracy and precision, were achieved through use of Rician noise model and Bayesian analysis as discussed in detail in the text.

Author Manuscript Author Manuscript Author Manuscript Author Manuscript

Author Manuscript Author Manuscript Author Manuscript Author Manuscript

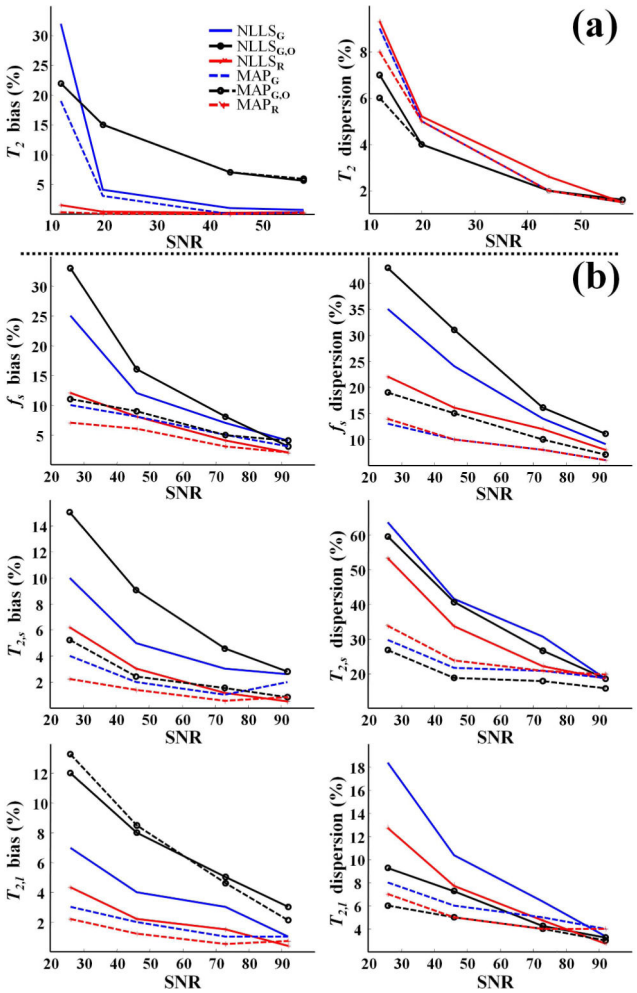

Fig. 6.

Phantom study results showing relative bias and dispersion in parameter estimates as a function of SNR using the fitting methods $NLLS_G$, $NLLS_{G,O}$, $NLLS_{\mathbf{R}}$, MAP_G, $MAP_{G,O}$ and $MAP_{\mathbf{R}}$. (a) Results for T_2, assuming the monoexponential signal model with T_2 = 58 ms as the underlying parameter value. (b) Results for f_s, $T_{2,s}$ and $T_{2,l}$ assuming the biexponential signal model with f_s = 0.33, $T_{2,s}$ = 14 ms and $T_{2,l}$ = 112 ms as underlying parameter values. Overall, accuracy and precision were substantially improved through use of Rician noise model and Bayesian analysis; see text for detailed discussion.

Author Manuscript Author Manuscript Author Manuscript Author Manuscript

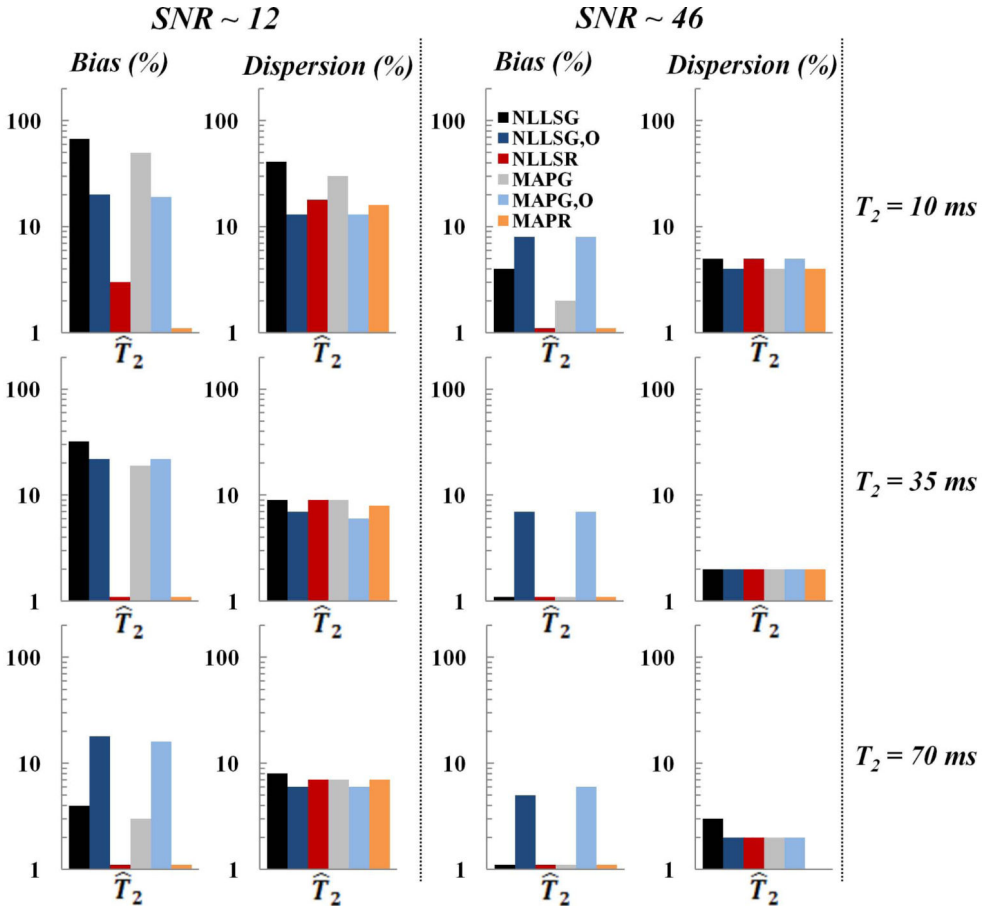

Fig. 7.

Relative bias and dispersion obtained from phantom measurements for the estimation of T_2, with a monoexponential signal model, for SNR of ~ 12 (left column) and ~ 46 (middle column), using $NLLS_G$, $NLLS_{G,O}$, $NLLS_{\mathbf{R}}$, MAP_G, $MAP_{G,O}$ and $MAP_{\mathbf{R}}$ analysis methods for three different input T_2 values (right column). Improvements in accuracy and precision are seen through use of Rician noise model and Bayesian analysis, as discussed in the text.

Author Manuscript Author Manuscript Author Manuscript Author Manuscript

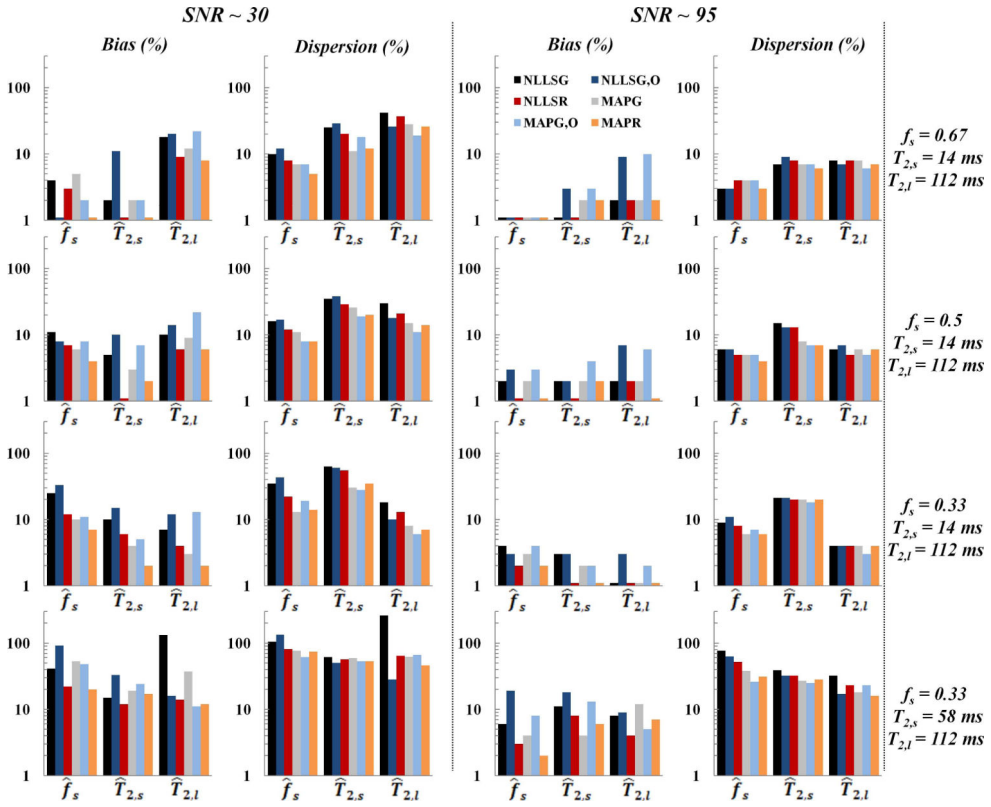

Fig. 8.

Relative bias and dispersion obtained from phantom measurements for the estimation of f_s, $T_{2,s}$ and $T_{2,l}$, with a biexponential signal model, for SNR of ~ 30 (left column) and ~ 95 (middle column), using $NLLS_G$, $NLLS_{G,O}$, $NLLS_{\mathbf{R}}$, MAP_G, $MAP_{G,O}$ and $MAP_{\mathbf{R}}$ analysis methods, for four different combinations of input f_s, $T_{2,s}$ and $T_{2,l}$ values (right column). Improvements in accuracy and precision are seen through use of Rician noise model and Bayesian analysis, as discussed in the text.

Author Manuscript Author Manuscript Author Manuscript Author Manuscript

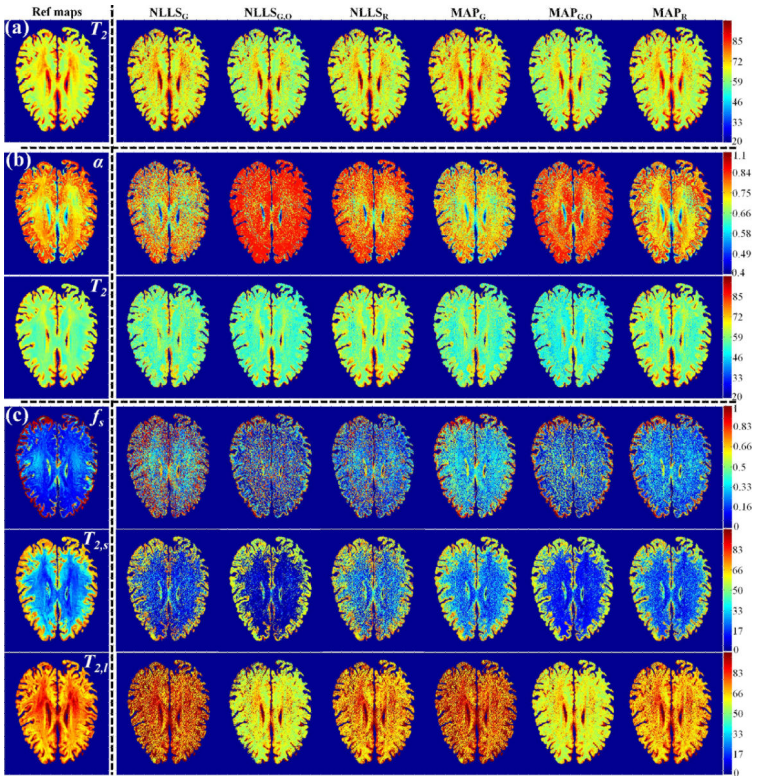

Fig. 9.

Reference parameter maps obtained at high SNR (~ 200) using the MAP$_{\mathbf{R}}$ method (left column) and parameter maps obtained at moderate SNR (~ 50) using the fitting methods NLLS$_G$, NLLS$_{G,O}$, NLLS$_{\mathbf{R}}$, MAP$_G$, MAP$_{G,O}$ and MAP$_{\mathbf{R}}$ (columns from left to right). (a) T_2 maps assuming the monoexponential signal model. (b) T_2 and α maps assuming the stretched exponential signal model. (c) f_s, $T_{2,s}$ and $T_{2,l}$ maps assuming the biexponential signal model. Greater consistency is achieved through use of Rician noise model and Bayesian analysis; see text for detailed discussion.

Author Manuscript Author Manuscript Author Manuscript Author Manuscript

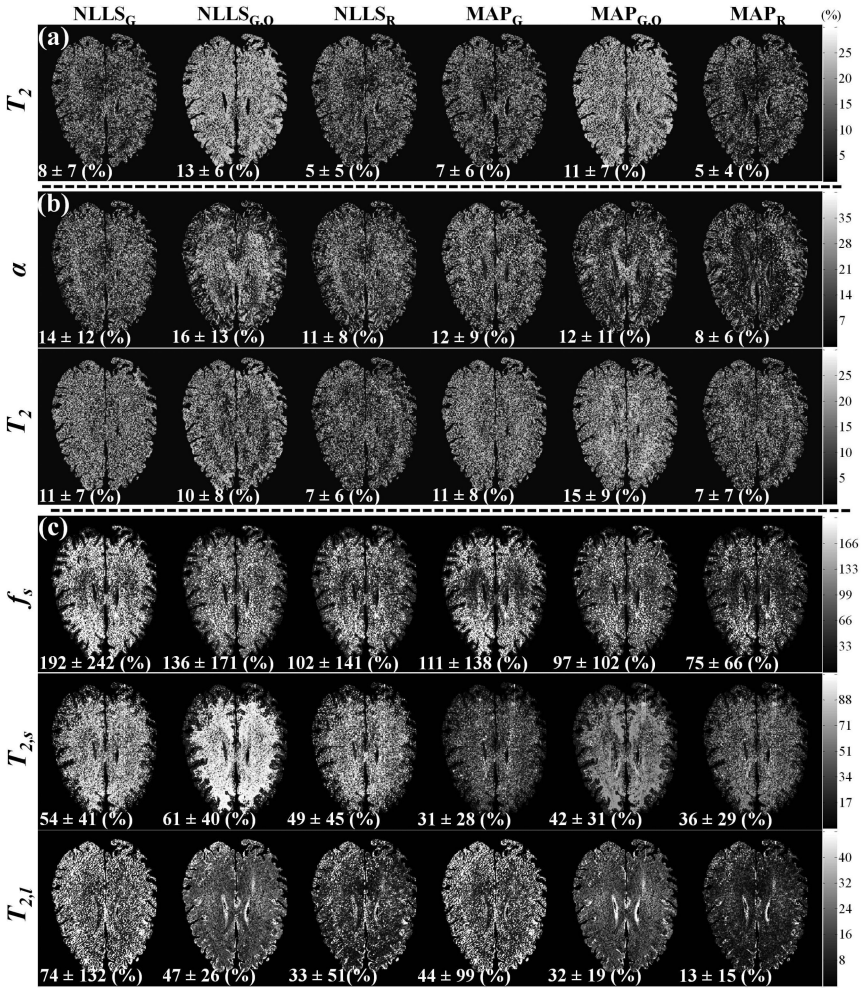

Fig. 10.

Relative error maps indicating the deviation of the parameter maps obtained at modest SNR (~ 50), shown in columns 2-7 of Fig. 9, from the high SNR fiducial map shown in column 1 of Fig. 9. The columns show the results obtained through use of NLLS$_G$, NLLS$_{G,O}$, NLLS$_{\mathbf{R}}$, MAP$_G$, MAP$_{G,O}$ and MAP$_{\mathbf{R}}$ for (a) the monoexponential signal model, (b) the stretched exponential signal model, and (c) the biexponential signal model. The mean and standard deviation of the relative error is given below each error map. Clear improvements are seen through use of Rician noise model and Bayesian analysis, as discussed in detail in the text.